PCCP

PAPER

View Article Online
View Journal | View Issue

Cite this: *Phys. Chem. Chem. Phys.*, 2018, **20**, 24641

n-Type Ohmic contact and p-type Schottky contact of monolayer InSe transistors†

Bowen Shi,[a] Yangyang Wang,*[b] Jingzhen Li,[a] Xiuying Zhang,[a] Jiahuan Yan,[a] Shiqi Liu,[a] Jie Yang,[a] Yuanyuan Pan,[a] Han Zhang,[a] Jinbo Yang,[ac] Feng Pan*[d] and Jing Lu*[ac]

Received 20th July 2018,
Accepted 7th September 2018

DOI: 10.1039/c8cp04615h

rsc.li/pccp

Owing to their few lateral dangling bonds and enhanced gate electrostatics, two-dimensional semiconductors have attracted much attention for the fabrication of channels in next-generation field-effect transistors (FETs). Herein, combining first-principle band structure calculations with more precise quantum transport simulations, we systematically explore the interface properties between monolayer (ML) indium selenide (InSe) and a sequence of common electrodes in an FET. The ML InSe band structure is damaged by Sc, Au, Cr, Pt, and Pd electrodes but identifiable in contact with Ag, Cu, In, graphene and ML O-terminated Cr_2C electrodes. A lateral n-type Schottky contact is generated with Sc, Au, Cr, Pt, Pd, and ML graphene electrodes owing to Fermi level pinning originating from the metal-induced gap states, which feature a pinning factor of 0.32. Luckily, a highly desirable lateral n-type Ohmic contact is generated with the Ag, Cu, and In electrodes. The calculated contact polarity is in agreement with the available experimental results using Au, Cr, ML graphene, Ag, and In as electrodes. Remarkably, a lateral p-type Schottky contact is generated with ML O-terminated Cr_2C despite the very high work function of ML InSe. Therefore, this study offers a deeper understanding of ML InSe device interfaces and instructions for the design of ML InSe transistors.

1. Introduction

Two-dimensional (2D) materials such as transition metals dichalcogenides[1,2] (TMDs), graphene,[3] silicene,[4] phosphorene,[5] arsenene,[6] stanene,[7] bismuthene,[8] and tellurene[9–11] have attracted tremendous attention for the fabrication of nanoscale electronic and optoelectronic devices. Their atomic thickness favors fantastic gate control, and their few dangling bonds at the interface benefit carrier transport.[12] However, TMDs have proper band gaps (1.0–2.0 eV)[13] but suffer from relatively low mobility (200 $cm^2\ V^{-1}\ s^{-1}$),[14] and thus are unsuitable for high performance applications.[15] Also, the absence of a band gap in graphene prevents its application in devices despite its superior carrier mobility (8390 $cm^2\ V^{-1}\ s^{-1}$).[16] Phosphorene has a high carrier mobility (1000 $cm^2\ V^{-1}\ s^{-1}$) and a moderate band gap (0.3–1.0 eV), but it easily decomposes in air.[5] Thus, the development of high carrier mobility and high stability 2D semiconductors is in high demand. Recently, a new 2D III–VI semiconductor, indium selenide (InSe), with a band gap of 1.52 eV for its monolayer (ML) and 0.69 eV for five layers[17] has attracted much attention.[18–24] It has been widely studied in optoelectronic applications owing to its novel optical properties.[18,19,25,26] Remarkably, the intrinsic electron mobility in multilayer InSe field-effect transistors (FETs) exceeds 10^3 $cm^2\ V^{-1}\ s^{-1}$ at room temperature.[20,27,28] Furthermore, InSe is more stable than phosphorene.[20,29] Thus, these two advantages make 2D InSe a competitive candidate as a channel material in next-generation electronics.[20,30]

When 2D semiconductors are used as channel materials, the channel is mostly directly contact with the metal to be doped owing to the lack of substitutional doping methods.[31,32] A finite Schottky barrier is often generated at the interface between the electrode and channel, which reduces the electron and hole injection efficiency. Therefore, the formation of low-resistance metal–2D semiconductor contacts, preferably Ohmic contacts, is a vital in the fabrication of devices. However, the Schottky barrier height (SBH) is not merely determined by the difference between the valence band maximum (VBM) or conduction band

[a] *State Key Laboratory of Mesoscopic Physics and Department of Physics, Peking University, Beijing 100871, P. R. China*
[b] *Nanophotonics and Optoelectronics Research Center, Qian Xuesen Laboratory of Space Technology, China Academy of Space Technology, Beijing 100094, P. R. China. E-mail: wangyangyang@qxslab.cn*
[c] *Collaborative Innovation Center of Quantum Matter, Beijing 100871, P. R. China. E-mail: jinglu@pku.edu.cn*
[d] *School of Advanced Materials, Peking University, Shenzhen Graduate School, Shenzhen 518055, P. R. China. E-mail: panfeng@pkusz.edu.cn*

† Electronic supplementary information (ESI) available: A schematic illustration of the SBH evolution from ML InSe to multilayer InSe. See DOI: 10.1039/c8cp04615h

minimum (CBM) of the intrinsic semiconducting 2D material and the Fermi level of the electrode owing to Fermi level pinning (FLP) at the semiconductor–metal interface. Thus, quantum transport simulations are necessary to accurately calculate the SBH in 2D FETs, which take electrode-channel coupling into account.[33–36]

Herein, we comprehensively study the electrical contacts of monolayer InSe transistors using Ag, Cu, In, Sc, Au, Cr, Pt, Pd, ML graphene, and ML O-terminated Cr_2C (O-Cr_2C) as electrodes based on first-principle band structure calculations and quantum transport simulations. No vertical Schottky barrier is generated at the ML InSe–metal interface owing to band hybridization (Sc/Au/Cr/Pt/Pd) and conduction band filling of ML InSe (Ag/Cu/In). However, a vertical n-type Schottky contact exists with the graphene electrode, which features an electron SBH of 0.01 eV. The quantum transport simulations reveal that Sc, Au, Cr, Pt, Pd, and graphene form lateral n-type Schottky contacts with ML InSe, which have electron SBH of 0.25, 0.35, 0.41, 0.54, 0.61, and 0.55 eV, respectively. Remarkably, Ag, Cu, and In form lateral n-type Ohmic contacts with ML InSe. The calculated Schottky contact type is consistent with the available experimental results using Ag, In, Cr, Au, and graphene as electrodes.[20,27,37,38] Only an n-type InSe–metal contact is reported in the previous experimental and theoretical studies due to the large work function of few-layer InSe. Thus, it is very important to form a p-type contact in complementary metal oxide semiconductor devices. We find that ML O-Cr_2C, with a very large work function, forms a p-type Schottky contact with ML InSe in both the vertical and lateral directions, which exhibits a hole SBH of 0.68 and 0.76 eV, respectively. The FLP exists in the lateral interface of ML InSe FETs owing to the metal-induced gap states (MIGS) featured by a pinning factor of 0.32, indicating strong coupling between the electrode and channel in ML InSe FETs.

2. Methodology

2.1. Interface modeling

We used ten types of materials Ag, Cu, In, Sc, Au, Cr, Pt, Pd, ML graphene, and ML O-Cr_2C as electrodes, which cover a large work function range. We placed ML InSe on the metal/ML graphene/ML O-Cr_2C surfaces as the electrode (Fig. 1(b)). Five-layer metal atoms were selected to simulate the bulk metal and the bottom two layers were fixed to simulate the internal atoms in the electrode based on previous studies.[39–41] The lattice parameters of InSe (a = b = 4.065 Å, as shown in Fig. 1(a)) was fixed to fit the metals/ML graphene/ML O-Cr_2C. ML InSe has a 1.52 eV indirect band gap without spin-orbital coupling (Fig. 1(c)), which is consistent with the former result of 1.44 eV at the density functional theory (DFT) level.[17] The lattice parameter, band structure and density of states of ML InSe are consistent with that from the previous theoretical study.[17] A vacuum space was set above 20 Å in the direction perpendicular to the surface between ML InSe and metals. The 1 × 1 ML InSe matches $\sqrt{3} \times \sqrt{3}$ Cu(111)/ML graphene. The $\sqrt{3} \times \sqrt{3}$ ML InSe matches 2 × 2 Sc(0001). The 2 × 2 ML InSe matches $\sqrt{7} \times \sqrt{7}$ Ag(111)/ML O-Cr_2C and 3 × 3 Au(111)/Pt(111)/Pd(111). The $2 \times \sqrt{3}$ ML InSe matches $\sqrt{5} \times \sqrt{5}$ In(110) and the $\sqrt{13} \times 1$ ML InSe matches $2\sqrt{7} \times \sqrt{3}$ Cr(110). The mismatch in these contact was less than 5%, as shown in Table 1.

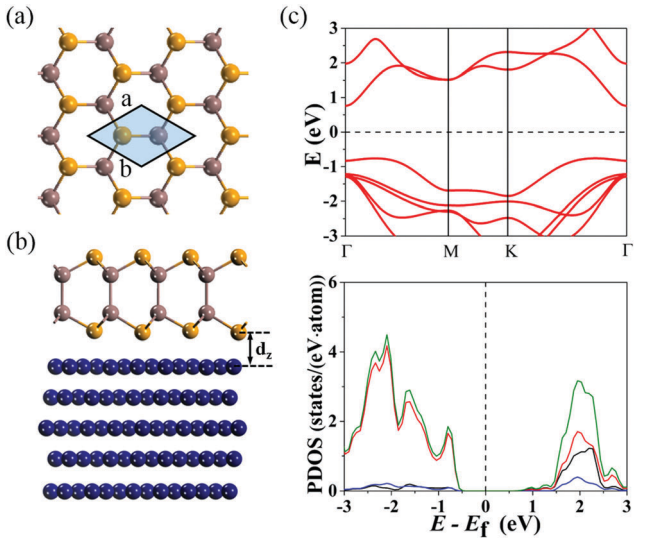

Fig. 1 (a) Top-view of freestanding ML InSe. Yellow and purple balls represent In and Se atoms, respectively, and the diamond indicates the unit cell of ML InSe. (b) Initial configuration of ML InSe on the metal surface (blue ball). (c) Band structure and partial density of states (PDOS) of intrinsic ML InSe. Black, red, blue, green lines represent s, p, d, and total orbitals, respectively.

2.2. Computational details

Calculations were based on the Vienna *ab initio* simulation package (VASP) code.[42–44] The projector-augmented wave (PAW) pseudopotential and a plane-wave basis set with a 500 eV cut-off energy were used in the calculation. The dipole correction eliminates the pseudo interaction generated by the periodic boundary condition in the vacuum direction and the DFT-D3 method takes the van der Waals (vdW) interaction into consideration. The k-point mesh for the relaxation and single-point calculation was sampled using the Monkhorst–Pack method with a mesh of 0.03 and 0.015 $Å^{-1}$ in the Brillouin zone, respectively. The maximum force and energy were converged to less than 2×10^{-2} eV $Å^{-1}$ per atom and 10^{-5} eV between two consecutive steps, respectively.

An FET with the ML InSe–metal compound system as the electrode and 5 nm ML InSe as the channel was constructed to simulate the properties of the electrode and channel interface (Fig. 2). Based on former results,[33,34,45] the observed SBHs of the electrode and channel interface in 2D semiconductor FETs are well reproduced by a 5 nm channel. The transport properties were calculated using the Atomistix ToolKit (ATK) 2016 package[46–48] based on DFT and non-equilibrium Green's function (NEGF) method. The transmission coefficient $T^{k_\parallel}(E)$ was calculated as follows: ($k_\parallel$ represents the reciprocal lattice vector parallel to the interface in the irreducible Brillouin zone (IBZ))

$$T^{k_\parallel}(E) = \mathrm{Tr}\left[\Gamma_{\mathrm{L}}^{k_\parallel}(E) G^{k_\parallel}(E) \Gamma_{\mathrm{R}}^{k_\parallel}(E) G^{k_\parallel\dagger}(E)\right] \quad (1)$$

Table 1 Calculated interfacial properties of ML InSe–metal contacts $\bar{\varepsilon}$ is the average lattice constant mismatch between the metal surfaces and ML InSe. The equilibrium distance, d_z, is the average distance between the contact ML InSe–metal interfaces in the vertical direction. $d_{\mathrm{InSe-M}}$ is the minimum atom-to-atom distance from the selenium atoms to the metal atoms. The binding energy, E_b, is the energy per indium selenide unit (In_2Se_2) required to remove ML InSe from the metal surface. W_M and $W_{\mathrm{InSe-M}}$ are the calculated work function for a clean metal surface and the ML InSe–metal system, respectively. $\Phi^{e}_{L,W}(\Phi^{h}_{L,W})$ and $\Phi^{e}_{L,T}(\Phi^{h}_{L,T})$ are the lateral electron (hole) SBHs obtained from the work function approximation and the quantum transport simulation, respectively. E^{T}_{g} is the transmission gap of the ML InSe FETs

Metal	Ag	Cu	In	Sc	Au	Cr	Pt	Pd	O-Cr_2C	Graphene
$\bar{\varepsilon}$ (%)	4.24	2.63	3.60	4.26	4.02	0.91	1.55	0.99	1.17	3.10
d_z (Å)	2.61	2.31	3.09	1.53	2.66	1.81	2.08	2.06	2.55	3.52
$d_{\mathrm{InSe-M}}$ (Å)	2.76	2.47	3.41	2.62	2.75	2.32	2.51	2.47	3.10	3.52
E_b (eV)	−0.72	−0.86	−0.36	−1.74	−0.77	−1.70	−1.10	−1.28	−0.30	−0.09
$W_{\mathrm{InSe-M}}$ (eV)	4.33	4.40	4.18	3.78	4.87	4.72	5.11	4.93	5.78	4.68
W_M (eV)	4.20	4.77	4.00	3.60	5.00	4.69	5.76	5.27	6.45	4.60
$\Phi^{e}_{L,W}$ (eV)	−0.28	−0.21	−0.43	−0.83	0.26	0.11	0.50	0.32	1.17	0.07
$\Phi^{e}_{L,T}$ (eV)	−0.04 (0.23)[a]	−0.02 (0.00)[a]	−0.01	0.25	0.35 (0.64)[a]	0.41	0.54	0.61	1.01	0.55
$\Phi^{h}_{L,W}$ (eV)	1.80	1.73	1.95	2.35	1.26	1.41	1.02	1.20	0.35	1.45
$\Phi^{h}_{L,T}$ (eV)	1.58	1.27	1.48	1.32	1.30	1.13	1.12	0.90	0.75	0.88
E^{T}_{g} (eV)	1.54	1.25	1.47	1.57	1.65	1.54	1.66	1.51	1.76	1.43

[a] From ref. 54.

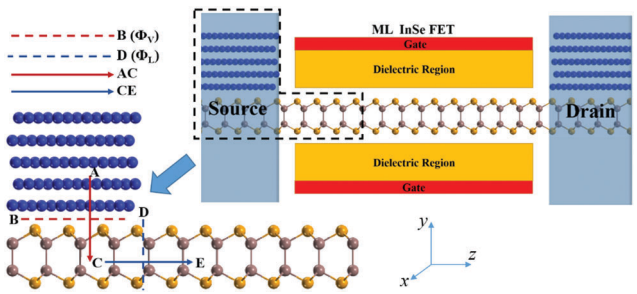

Fig. 2 Right: Schematic diagram of an ML InSe transistor. Left: Schematic cross-sectional view of a typical metal contact with the intrinsic ML InSe channel. A, C, and E are the three charge transfer (electron/hole-transfer) regions. B and D are the source/drain interface (red dashed line) and the source/drain-channel interface D (blue dashed lines), respectively. Φ_V and Φ_L represent the vertical SBH and lateral SBH, respectively. Yellow and purple balls represent In and Se atoms, respectively. The *x*, *y*, and *z* axes are the period direction, direction vertical to the ML InSe plane, and direction along the channel length, respectively.

where, the gamma function $\Gamma^{k_\parallel}_{L/R}(E) = i\left(\sum_{L/R}^{r,k_\parallel} - \sum_{L/R}^{a,k_\parallel}\right)$ represents the level broadening stemming from left and right electrodes. $\sum_{L/R}^{k_\parallel}$ represents the self-energy of the left/right junction. $G^{k_\parallel}$ is the retarded (advanced) Green's function. The transmission function at a specified energy $T(E)$ was obtained by averaging all the different $k_\parallel$ in the IBZ. According to our former calculation,[49] the single-ξ polarized (SZP) basis set is often sufficiently accurate for bulk metal electrode systems. However after testing, we found that for ML graphene and O-Cr_2C electrodes, the double-ξ polarized (DZP) basis set is required. The temperature was set at 300 K to simulate the environment. A Monkhorst–Pack of 50 × 1 × 1 and 50 × 1 × 50 *k*-point grids was adopted to simulate the electronic structures of the central region and the electrodes, respectively.

A generalized gradient approximation (GGA) of the Perdew–Burke–Ernzerhof (PBE) form was employed throughout.[50] In a heavily doped semiconductor, its electron behavior, especially its band gap, can be approximately depicted by DFT-GGA. For instance, the band gap of a degenerately doped ML $MoSe_2$ at the DFT-GGA level is 1.53 eV, which is in accord with the renormalized band gap of 1.59 eV obtained by the GW method and experimental result of 1.58 eV.[51] Since doped carriers from the electrode highly screen the electron–electron interaction in FET, we adopted DFT-GGA to evaluate the SBH.[51,52] Specifically, the single electron approximation is sufficiently effective to describe the electron behavior in an FET. For instance, the experimental transport gap of ML, bilayer (BL), and trilayer (TL) black phosphorene with Ni as the electrode is 0.99, 0.71, and 0.61 eV,[53] respectively. The result of the transport gap for the same system at the DFT-GGA level is 0.79, 0.81, and 0.68 eV, respectively, in terms of the LDDOS at the interface.[34–36] The root cause of the discrepancy may come from two reasons. One is that defects always exist in the actual sample, which cause FLP and affect the SBH. However, in our model, no defect was considered, and this ignorance will lead to uncertainty. The other is that the many-body effect remains, which is not fully captured by DFT-GGA although it is greatly depressed in an FET. In addition, the calculated electron (hole) SBH in the ML/BL/TL phosphorene FET with an Ni electrode is 0.39/0.52/0.48 (0.26/0.19/0.20) eV[34–36] at the DFT-GGA level, which is consistent with the observed value of 0.64/0.48/0.40 (0.35/0.23/0.21) eV.[53]

3. Results and discussion

3.1. Electronic band structure calculations

The optimized ML InSe–metal/ML graphene/ML O-Cr_2C contact configurations are shown in Fig. 3. The structure of ML InSe changes slightly on the Ag, Cu, In, Au, Pt, Pd, ML graphene, and ML O-Cr_2C surfaces and strongly on the Sc and Cr surfaces. The equilibrium distance, d_z, is the distance in the vertical direction between InSe and the closest metal layer (Fig. 1(b)), and $d_{\mathrm{InSe-M}}$ is the closest distance between the selenium atom and the

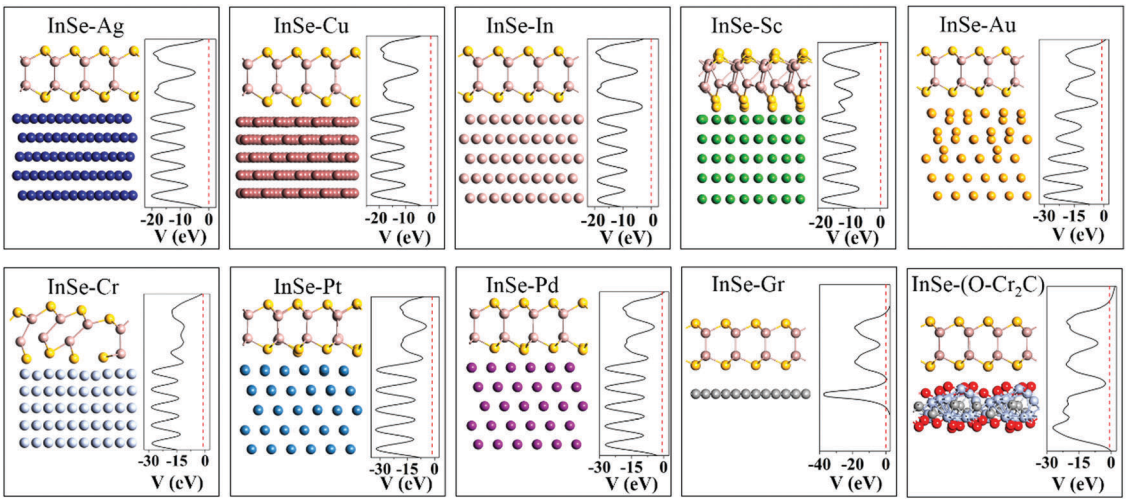

Fig. 3 Side-view of the optimized structures and average electrostatic potential distributions in the planes normal to the interface of ML InSe on Ag, Cu, In, Sc, Au, Cr, Pt, Pd, ML graphene, and ML O-Cr_2C surfaces, respectively. Yellow and purple balls represent In and Se atoms, respectively. At the interface of ML InSe on ML O-Cr_2C, the red, gray, and light blue balls represent O, C, and Cr atoms, respectively. The Fermi level is set to zero.

metal/carbon/oxygen atom. The binding energy E_b of the ML InSe–metal/ML graphene/ML O-Cr_2C system is defined as:

$$E_b = (E_{InSe} + E_M - E_{InSe-M})/N$$

where, E_{InSe}, E_M, and E_{InSe-M} represent the binding energy of the pristine InSe, metal and electrode, respectively. N is the total number of $(InSe)_2$ in the system, which for $(InSe)_2$ is the basic unit of the ML InSe structure. The relevant parameters of the ML InSe–metal/ML graphene/ML O-Cr_2C systems are presented in Table 1. The interaction between ML InSe and the metal/ML graphene/ML O-Cr_2C surface can be divided into three classes based on the binding energy, E_b, equilibrium distance, d_z, and the closest distance between the selenium atom and the electrode atom, d_{InSe-M}. The first group is ML InSe on the ML graphene/ML O-Cr_2C/In with vdW interaction, which is characterized by a small E_b (−0.09 to −0.36 eV), and large distance d_z (2.55–3.52 Å) and d_{InSe-M} (2.83–3.52 Å). The second group is ML InSe on Ag/Cu/Au surface with moderate interaction, which features a medium E_b (−0.72 to −0.86 eV), d_z (2.31–2.66 Å) and d_{InSe-M} (2.47–2.76 Å). The third group is ML InSe on Sc/Cr/Pt/Pd surface with strong interaction, which is characterized by a large E_b (−1.10 to −1.74 eV), and small d_z (1.53–2.08 Å) and d_{InSe-M} (2.32–2.62 Å).

The differences between the bond strength in the latter two groups are due to the difference in the number of covalent bonds between ML InSe and the metals. The isolated Ag ($4d^{10}5s^1$)/Cu ($3d^{10}4s^1$)/Au ($5d^{10}6s^1$) atoms have one unpaired s electron in their outermost orbit, thus one covalent bond is formed with ML InSe, which corresponds to a smaller E_b. The isolated Sc ($3d^14s^2$)/Cr ($3d^54s^1$)/Pt ($5d^96s^1$)/Pd ($4d^{10}$) atoms have one/six/two/zero unpaired electrons in their outer orbits, respectively. When these atoms are in the solid form, the nd and (n + 1)s electrons undergo a redistribution due to the orbital overlap. The electronic configuration of bulk Sc and Pd can be approximatively expressed as $3d^24s^1$ and $4d^95s^1$ considering the respective Mulliken population analysis results of $3d^{1.6}4s^{1.4}$ and $4d^{9.3}5s^{0.7}$, respectively. Accordingly, Sc/Cr/Pt/Pd provides three/six/two/two unpaired electron to form covalent bonds with ML InSe, which correspond to a larger E_b.

To analyze the electrical properties in the ML InSe–metal/ML graphene/ML O-Cr_2C contacts, the band structures of the contacts were determined, as displayed in Fig. 4, which are consistent with the previous experimental results.[22,23] The ML InSe band structure is almost intact in contact with graphene and ML O-Cr_2C owing to the weak vdW interaction. The band structure of ML InSe is slightly hybridized and identifiable on Ag/Cu/In owing to the weak covalent bonding or strong vdW interaction (In). Also, in the case of the InSe–Ag, Cu, In, ML graphene, and ML O-Cr_2C systems, their band structure is identifiable. (Namely, the band structure of the InSe-projected bands in the electrodes is basically the same as that of the intrinsic InSe). A vertical Ohmic contact is formed in the InSe–Ag, Cu, In, and ML graphene systems, and a vertical Schottky contact is formed in the InSe-ML O-Cr_2C system. Since ML InSe has a large work function (5.37 eV), the Fermi level of this system is above the CBM of the ML InSe in ML InSe–Ag/Cu/In and ML graphene systems, implying electron doping in ML InSe. The conduction band filling of ML InSe on Ag, Cu, In and ML graphene in terms of carrier density is approximately 4.1×10^{14}, 2.2×10^{14}, 1.1×10^{14}, and 2.2×10^{14} electrons per cm^2, respectively. Thus, ionic interactions exist in the three interfaces in addition to weak covalent/strong vdW interactions. The band structure is strongly destroyed on Au/Sc/Cr/Pt/Pd due to the strong covalent interaction, suggesting the metallization of ML InSe. The band structure is unidentifiable and InSe is metallized, thus the Schottky contact cannot exist. In general, the hybridization degree of the ML InSe band structure on different metal surfaces is consistent with their binding strength.

The partial density of states (PDOS) of the ML InSe–metal/ML graphene/ML O-Cr_2C systems projected in ML InSe are shown in Fig. 5. The states around the Fermi level are predominantly

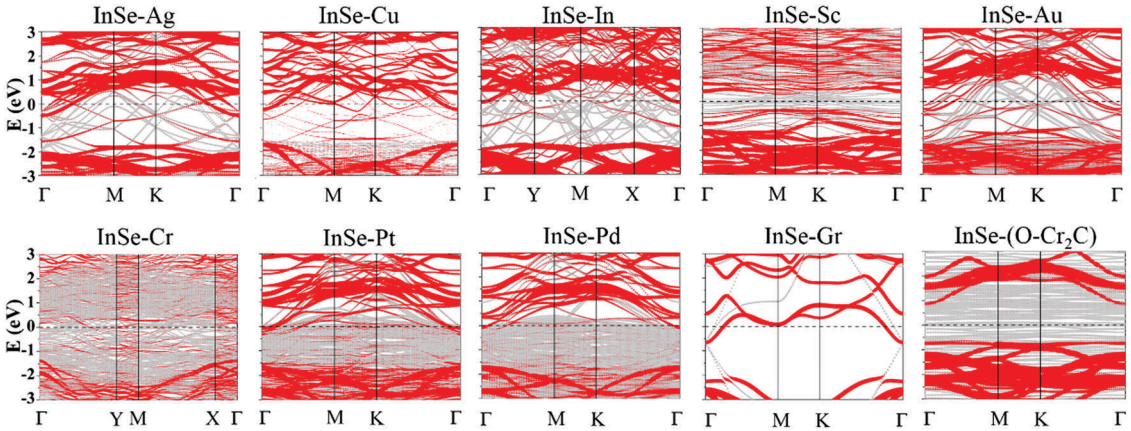

Fig. 4 Band structures of the ML InSe–metals/ML graphene/ML O-Cr_2C systems. Gray line: band structures of the interfacial system and Red line: band structures projected to ML InSe. The Fermi level is set to zero energy and is denoted by the dashed line.

p orbitals, which is in agreement with the outmost electronic structure of In ($5s^25p^1$) and Se ($4s^24p^4$). The ML InSe band gap disappears in all the ML InSe–metal systems as a result of hybridization of ML InSe. In the ML InSe–ML graphene system, the ML InSe band gap is preserved well. However for ML O-Cr_2C, there is a small amount of states around the Fermi level, which are identified as MIGS. The PDOS of the latter two systems are in agreement with the weak vdW interaction.

To further assess the interaction of ML InSe–metal/ML graphene/ML O-Cr_2C interface, we plotted the electron localization function of the compound systems in Fig. 6. There is no significant electron cumulation in the interface with In, ML graphene, and ML O-Cr_2C, in agreement with the small E_b (−0.09 to −0.36 eV) and vdW interaction. Electrons are slightly accumulated in the interface with Ag, Cu, and Au, in agreement with the moderate E_b (−0.72 to −0.86 eV). The electron density distribution is strongly accumulated at the interface with Sc, Cr, Pt, and Pd, in agreement with the large E_b (−1.10 to −1.74 eV) and strong covalent bonding.

3.2. Vertical and lateral SBH of the ML InSe transistors

The Schottky barrier plays an important role in FETs. A low Schottky barrier will decrease the scattering of carriers, increase the carrier mobility, and improve the property of a transistor. A schematic diagram of a 5 nm-channel ML InSe FET is displayed in Fig. 2. Two types of Schottky barrier possibly exist in the FET. One is the vertical Schottky barrier, Φ_V, at interface B (between the ML InSe and the metal/ML graphene/ML O-Cr_2C) in the vertical direction, and the other is the lateral Schottky barrier, Φ_L, at interface D (between the ML InSe channel and the electrode) in the lateral direction. The electron/hole SBH is calculated from the difference between the CBM/VBM of ML InSe and the Fermi level at interface D. The metallization of ML InSe on Sc, Au, Cr, Pt, and Pd eliminates the vertical Schottky barrier at interface B, while the conduction band filling of ML InSe on Ag, Cu, In, and ML graphene results in a vertical n-type Ohmic contact at interface B. However, when ML InSe is contacted with ML O-Cr_2C, the band structure is identifiable (Fig. 4).

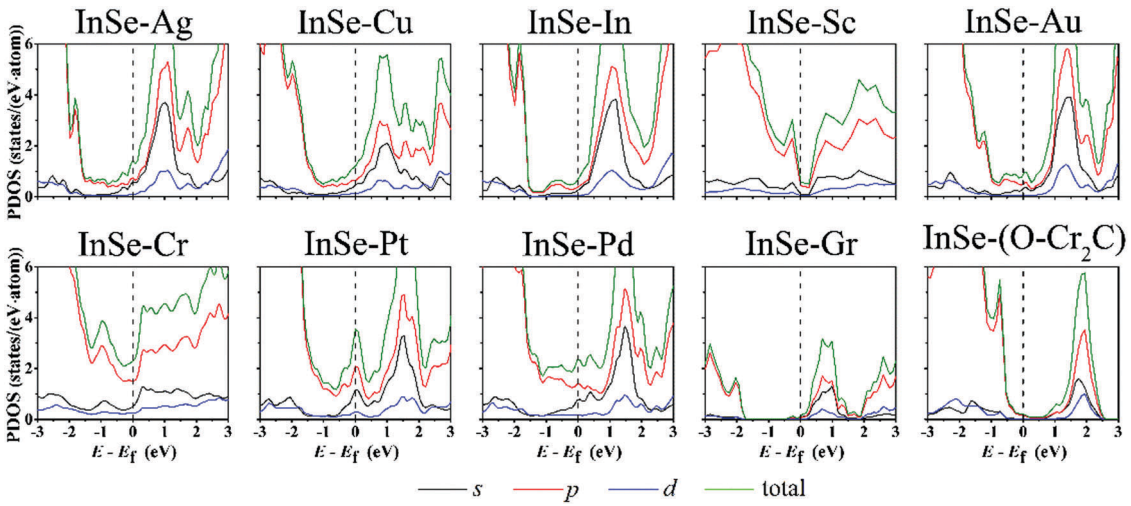

Fig. 5 Partial density of states (PDOS) of ML InSe on the metal/ML graphene/ML O-Cr_2C surfaces. The Fermi level is set to zero energy and is denoted by the dashed lines.

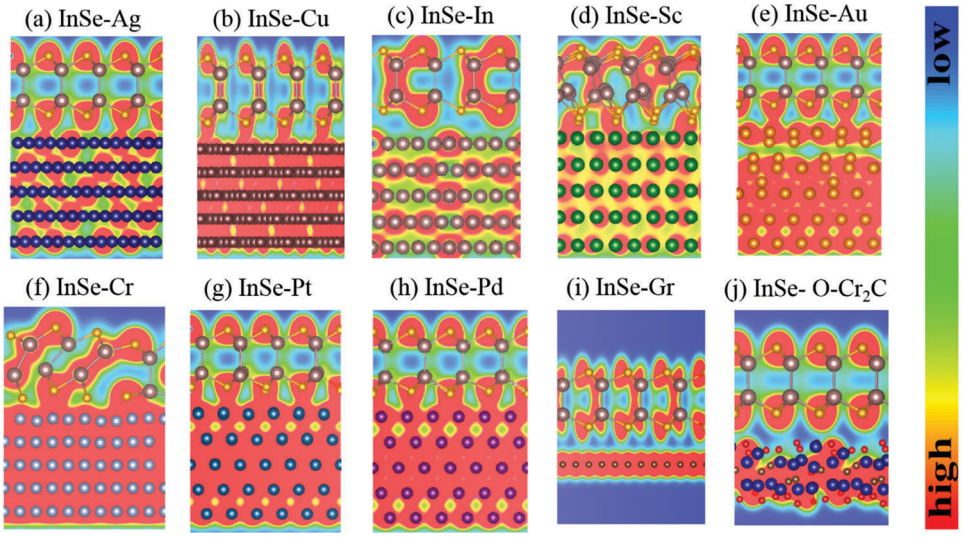

Fig. 6 Total electron density distributions of ML InSe in contact with (a) Ag, (b) Cu, (c) In, (d) Sc, (e) Au, (f) Cr, (g) Pt, (h) Pd, (i) ML graphene, and (j) ML O-Cr_2C. Yellow and purple balls represent In and Se atoms, respectively.

A vertical p-type Schottky contact is generated, which features a hole SBH of 0.68 eV.

If the band structure of ML InSe can be identified in the electrode region (Ag, Cu, In, ML graphene, and ML O-Cr_2C systems), we can also obtain the vertical SBH from the LDDOS (Fig. 7). The vertical electron/hole SBH is defined as the difference between the CBM/VBM of ML InSe and the Fermi level in the deep electrode part (far away from the channel). For Ag, Cu, and In, a vertical n-type Ohmic contact is obtained from the LDDOS, which is in agreement with the result for the band structure (Fig. 4). However, in the ML graphene system, a vertical Ohmic contact is obtained from the band structure (Fig. 4), while a Schottky vertical contact is obtained from the LDDOS at the interface (Fig. 7(i)). The reason for the difference is that the CBM/VBM (represented by black line) of ML InSe is bent downwards in the electrode region due to the electron transfer from the electrode to the channel. As a result, the vertical SBH decreases as it moves toward the electrode direction. If the electrode region is long enough, an n-type Ohmic contact is expected in the LDDOS, which is in agreement with the band structure calculation. If the electrode region is long enough, an n-type Ohmic contact is expected in the LDDOS. For ML O-Cr_2C, a vertical p-type Schottky contact is obtained from the LDDOS with a height of 0.69 eV, which is consistent with the value obtained from the band structure (0.68 eV).

There are two methods to calculate the lateral SBH. One is the work function approximation (WFA) and the other is the first-principle quantum transport calculation. In the WFA, the difference between the CBM (VBM) of the intrinsic InSe and the Fermi level of the ML InSe–metal/ML graphene/ML O-Cr_2C system determines the lateral electron (hole) SBH. At the WFA level, a lateral n-type Ohmic contact is generated between ML InSe and Sc, In, Ag, and Cu. A lateral n-type Schottky contact is generated between ML InSe and Cr, ML graphene, Au, Pd, and Pt, which features electron SBHs of 0.11, 0.21, 0.26, 0.32, and 0.50 eV, respectively. ML O-Cr_2C forms a lateral p-type Schottky contact with ML InSe, featuring a hole SBH of 0.35 eV. The lateral SBH results of the WFA are shown in blue in Fig. 8(a). In the WFA, electrode-channel coupling is neglected.

To take the electrode-channel coupling into consideration, the first-principles quantum transport calculation was used to ascertain the lateral SBH. In the first-principles quantum transport calculation, the lateral electron (hole) SBH is quantitatively described by the difference between the CBM (VBM) and the Fermi level at the lateral interface D (Fig. 2) attained from the LDDOS. If the lateral electron (hole) SBH is different in the left and right interface, we take the average SBH of the left and right interface. (The reason for the difference in the left and right interface is due to the asymmetric crystal surface structure in the transmission direction.) This method has been verified using ML, BL, and TL black phosphorus FETs with an Ni electrode.[53] The lateral hole SBHs (0.20/0.19/0.26 eV) from in the quantum transport calculation agree with the observed hole SBHs (0.21/0.23/0.35 eV) in TL/BL/ML black phosphorus FETs. There is an ~30% difference between the calculated value of 0.26 eV and observed 0.35 eV. We should point out that firstly, the observed values of SBH may be different among different experiments. For example, the electron SBHs in an MoS_2 FET using Ti as the electrode are 0.18, 0.25, and 0.26 eV in different devices, where there is an ~30% difference between 0.18 eV and 0.26 eV.[44] Secondly, defects always exist in actual samples, which cause FLP and affect the SBH, but in our model, no defect was considered, and this ignorance will lead to uncertainty. Thirdly, the many-body effect remains and is not fully captured by DFT-GGA although it is greatly depressed in an FET. Overall, the ~30% difference between the calculated 0.26 eV and observed 0.35 eV is not considered as a significant difference. Thus far, there is no qualitative discrepancy with the contact polarity and type between the *ab initio* quantum simulation and experiment for the examined 2D semiconductors.[33–36] Nevertheless, the

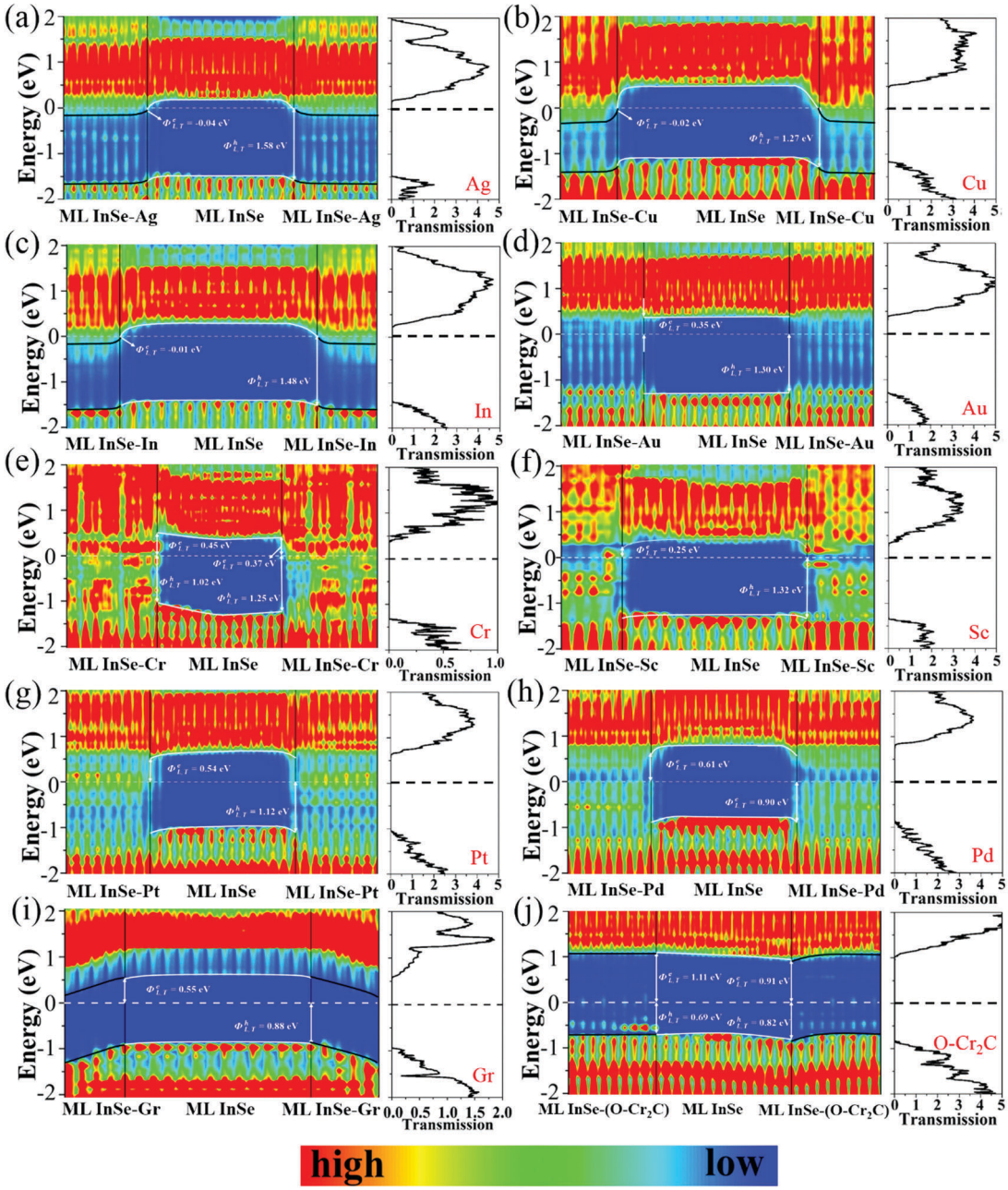

Fig. 7 (a)–(j) Zero-bias and zero-gate voltage LDDOS and transmission spectra of the ML InSe transistor with a channel length of L = 5 nm. The CBM and VBM in the channel region are represented by white lines. The CBM and VBM in the electrode region are represented by black lines. The Fermi level is represented by a white dash line in the LDDOS or a black dash line in the transmission spectra. $\Phi^{e}_{L,T}$ and $\Phi^{h}_{L,T}$ represent the electron SBH and hole SBH in the lateral direction, respectively. The upright black lines indicate the boundary of the ML InSe–bulk metal and the intrinsic ML InSe channel.

lateral hole SBHs (0.02/−0.10/−0.28 eV) of ML/BL/TL black phosphorus FETs obtained from the WFA are apparently different from the experimental results. Thus, it is crucial to take the electrode-channel coupling into consideration in order to reproduce the measured SBH.

The ML InSe FETs LDDOS and transmission spectra using the first-principle quantum transport calculation are depicted in Fig. 7. From the LDDOS, Sc, Au, Cr, Pt, Pd, and graphene generate n-type Schottky contacts with ML InSe, which feature lateral electron SBHs of 0.25, 0.35, 0.41, 0.54, 0.61, and 0.55 eV, respectively. Remarkably, Ag, Cu, and In form highly desirable n-type Ohmic contacts with ML InSe. In a recent quantum transport simulation, Cu also generated an n-type Ohmic contact with ML InSe, but Ag generated an n-type Schottky contact with ML InSe, featuring an electron SBH of 0.23 eV, and Au forms an n-type Schottky contact with a slightly higher electron SBH of 0.64 eV (*vs.* 0.41 eV in this work).[54] Ag has a lower work function (4.20 eV) than Cu (4.77 eV), thus Ag tends to form a lower n-type SBH than Cu. In this regard, our result appears more reasonable. In that article, the hybrid functional

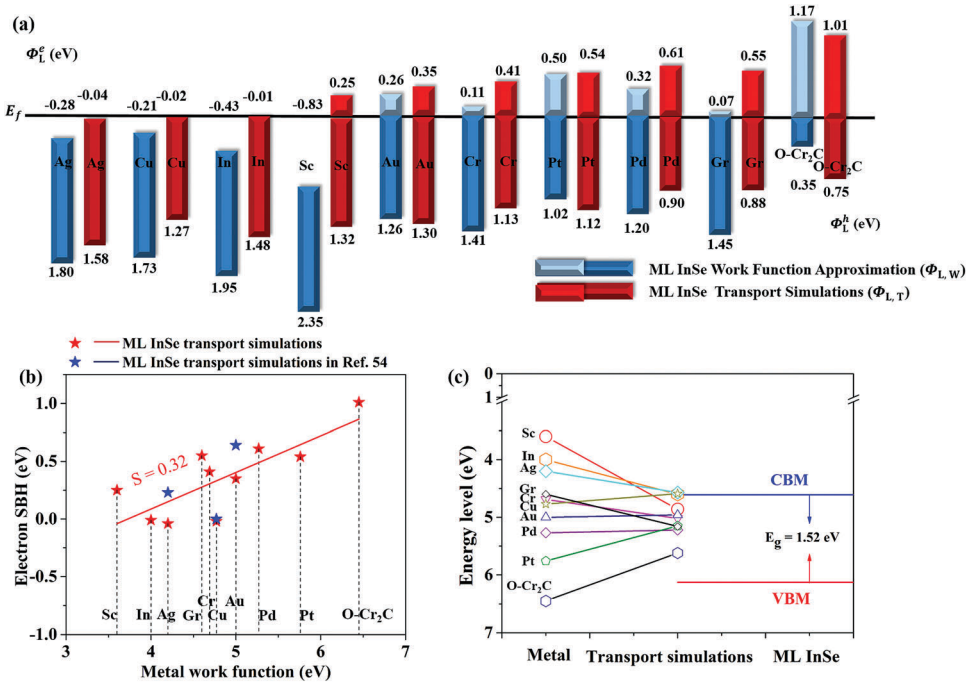

Fig. 8 (a) Comparison of the lateral SBHs obtained from the WFA and the quantum transport simulations for the ML InSe transistors. (b) Variation in the lateral electron SBHs for the ML InSe transistors with the bulk metal/ML graphene/ML O-Cr_2C work function. S is the pinning factor obtained from the Schottky–Mott rule. (c) Illustration of FLP in the ML InSe transistor.

(HSE06) was used, which always overestimates the transport gap because the channels in FETs often work in heavily doped states, and heavy doping significantly decreases the intrinsic band gap.[51,52] Therefore, as mentioned in the computational details section,[34–36,51,53] our results using the GGA method appear more reliable.

In our calculation, the lateral contact polarity obtained from the WFA is same as that from the quantum transport simulation. However, the contact type in the Sc contact with ML InSe is different between the two methods. The WFA gives a lateral n-type Ohmic contact, while the quantum transport simulation gives a lateral n-type Schottky contact with an electron SBH of 0.25 eV. Besides, the WFA underestimates the electron SBH for metals/graphene and underestimates the hole SBH for ML O-Cr_2C compared with the quantum transport simulation. The calculated contact type for ML InSe is consistent with the available observed data with Ag, In, Cr, Au, and graphene as electrodes for multilayer InSe.[20,27,37,38] Furthermore, the experiment shows that In forms a lower n-type SBH than Cr for multilayer InSe,[38] which is consistent with our calculation for ML InSe. Since multilayer InSe is constructed by monolayer InSe with weak vdW interaction,[9] the band gap center of multilayer InSe is approximately equal to that of monolayer InSe if the broadening of the valence band maximum and the conduction band minimum are equal to each other (Fig. S1, ESI†). Actually, according to our calculation, the band gap centers of ML (5.37 eV) and bilayer InSe (5.30 eV) are quite close to each other. Hence, the contact polarity and the relative relation of SBH are basically independent of the layer number, and these results obtained in ML InSe remain valid in multilayer InSe. Thus, it is reasonable to compare our theoretical results with the published experimental results.

Only n-type InSe–metal contacts are reported in the previous experimental[20,27,37,38] and theoretical[17,54] studies. In the Schottky–Mott limit, a large work function material will help form an n-type contact and prevent the formation of a p-type contact. Due to the large work function of ML and few-layer InSe, it is extremely difficult to obtain a p-type contact, and to the best of our knowledge, the ML InSe and O-terminated Cr_2C contact is the first p-type contact. We admit it is a rather weak p-type Schottky contact, and a strong p-type Schottky contact should be the goal of future work. It is very important to form a p-type contact in complementary metal oxide semiconductor devices. Remarkably, a p-type Schottky contact is generated in both the vertical and lateral directions, which feature hole SBHs of 0.68/0.69 (band structure/LDDOS) and 0.76 eV, respectively. The difference between the vertical and lateral directions is the result of the bending of the band structure (Fig. 7(j)).

The quantum transport calculation takes the coupling between the electrode and channel into consideration, and this coupling generates the FLP effect. The intensity of FLP is quantitatively described by the pinning factor S, which is defined as the slope of the fitted red line (Fig. 8(b)) and describes the change in the electron SBH with the work function of the electrode materials. According to this definition, S = 1 represents no FLP and S = 0 represents complete FLP. We obtained S = 0.32 in the ML InSe–metal lateral interface, which is comparable with the calculated values in ML MoS_2 (S = 0.27),[33] ML black phosphorene (S = 0.28),[34] ML arsenene (S = 0.33),[55,56] and ML blue phosphorene (S = 0.42).[57] This value

indicates strong FLP between the electrode and channel in the ML InSe transistor. The metalized ML InSe induces new states in the gap of channel ML InSe, namely MIGS. The MIGS serve as a partially filled container of electrons, which can accept or donate electrons and fix the Fermi level to the MIGS.

Our study suggests that ML InSe prefers n-type Schottky contacts with electrodes owing to its large work function of 5.37 eV, which is larger than that calculated (4.57 eV) for ML black phosphorene.[34] ML black phosphorene prefers p-type Schottky contacts with metals both experimentally and theoretically.[34,58] Ohmic contacts have a low contact resistance, which favors a high on-current and high-frequency operation in transistors.[59] However, it is difficult to form Ohmic contacts in 2D transistors. ML black phosphorene only forms a p-type hole SBH of 0.1 eV using graphene as the electrode in theory.[34,60] No Ohmic contact is generated with ML blue phosphorene.[57] Fortunately, in our study, ML InSe generates an n-type Ohmic contact with Ag, Cu, and In. Although ML InSe prefers n-type Schottky contacts, we find that ML O-Cr_2C, a high work function metallic carbide, forms a p-type contact with InSe, which is vital in complementary metal oxide semiconductor devices.

The transport gap, E_g^T, is the sum of the lateral electron and hole SBH in the quantum transport simulation, that is $E_g^T = \Phi_{L,T}^e + \Phi_{L,T}^h$. The E_g^T of the ML InSe transistor with Ag, Cu, In, Sc, Au, Cr, Pt, Pd, graphene, and ML O-Cr_2C is 1.54, 1.25, 1.47, 1.57, 1.65, 1.54, 1.66, 1.51, 1.72, and 1.76 eV, respectively, as shown in Table 1. These values are consistent with the intrinsic ML InSe band gap of 1.52 eV at the DFT-GGA level owing to doping.

4. Conclusion

In conclusion, we comprehensively studied the contact properties in ML InSe FETs using bulk metals, ML graphene and ML O-Cr_2C as electrodes. First-principle electronic structure calculations and quantum transport simulation were adopted herein. The metallization of ML InSe on Sc/Au/Cr/Pt/Pd leads to the absence of a vertical Schottky barrier, and the conduction band filling of ML InSe on Ag/Cu/In/graphene results in a vertical n-type Ohmic contact. Due to the strong FLP at the lateral interface of the ML InSe FETs due to the MIGS, Sc, Au, Cr, Pt, Pd, and ML graphene form a lateral n-type Schottky contact with ML InSe, featuring electron SBH of 0.25, 0.35, 0.41, 0.54, 0.61, and 0.55 eV, respectively, using first-principle quantum transport simulations. The fitted pinning factor is 0.32. Remarkably, Ag, Cu, and In form a lateral n-type Ohmic contact with ML InSe. For the first time, a p-type Schottky contact in both the vertical and lateral directions is generated with ML InSe on ML O-Cr_2C, which features a hole SBH of 0.68 and 0.76 eV, respectively, compensating for the absence of a p-type contact. This study provides a deep understanding of ML InSe–metal interfaces and instructions for the design of ML InSe-based devices.

Conflicts of interest

There are no conflicts of interest to declare.

Acknowledgements

This work was supported by the National Natural Science Foundation of China (No. 11674005/11664026/11704406) and the Ministry of Science and Technology of China (No. 2016YFB0700600 (National Materials Genome Project)/ 2016YFA0301300).

References

1 B. Radisavljevic, A. Radenovic, J. Brivio, V. Giacometti and A. Kis, Single-layer MoS_2 transistors, *Nat. Nanotechnol.*, 2011, **6**(3), 147–150.
2 Y. Pan, S. Li, M. Ye, R. Quhe, Z. Song, Y. Wang, J. Zheng, F. Pan, W. Guo, J. Yang and J. Lu, Interfacial Properties of Monolayer MoS_2-Metal Contacts, *J. Phys. Chem. C*, 2016, **120**(24), 13063–13070.
3 A. K. Geim and K. S. Novoselov, The rise of graphene, *Nat. Mater.*, 2007, **6**(3), 183–191.
4 Z. Ni, Q. Liu, K. Tang, J. Zheng, J. Zhou, R. Qin, Z. Gao, D. Yu and J. Lu, Tunable Bandgap in Silicene and Germanene, *Nano Lett.*, 2012, **12**(1), 113–118.
5 M. Z. Rahman, C. W. Kwong, K. Davey and S. Z. Qiao, 2D phosphorene as a water splitting photocatalyst: fundamentals to applications, *Energy Environ. Sci.*, 2016, **9**(3), 709–728.
6 Y. Wang, P. Huang, M. Ye, R. Quhe, Y. Pan, H. Zhang, H. Zhong, J. Shi and J. Lu, Many-body Effect, Carrier Mobility, and Device Performance of Hexagonal Arsenene and Antimonene, *Chem. Mater.*, 2017, **29**(5), 2191–2201.
7 Y. Guo, F. Pan, M. Ye, Y. Wang, Y. Pan, X. Zhang, J. Li, H. Zhang and J. Lu, Interfacial properties of stanene-metal contacts, *2D Mater.*, 2016, **3**, 3.
8 Y. Guo, F. Pan, M. Ye, X. Sun, Y. Wang, J. Li, X. Zhang, H. Zhang, Y. Pan, Z. Song, J. Yang and J. Lu, Monolayer Bismuthene-Metal Contacts: A Theoretical Study, *ACS Appl. Mater. Interfaces*, 2017, **9**(27), 23128–23140.
9 Y. Wang, G. Qiu, R. Wang, S. Huang, Q. Wang, Y. Liu, Y. Du, W. A. Goddard, M. J. Kim, X. Xu, P. D. Ye and W. Wu, Field-effect transistors made from solution-grown two-dimensional tellurene, *Nat. Electron.*, 2018, **1**(4), 228–236.
10 Z. Zhu, X. Cai, S. Yi, J. Chen, Y. Dai, C. Niu, Z. Guo, M. Xie, F. Liu, J. H. Cho, Y. Jia and Z. Zhang, Multivalency-Driven Formation of Te-Based Monolayer Materials: A Combined First-Principles and Experimental study, *Phys. Rev. Lett.*, 2017, **119**(10), 106101.
11 J. Yan, X. Zhang, Y. Pan, J. Li, B. Shi, S. Liu, J. Yang, Z. Song, H. Zhang and M. Ye, Monolayer Tellurene—Metal Contacts, *J. Mater. Chem. C*, 2018, **6**, 6153–6163.
12 J. Kang, W. Liu, D. Sarkar, D. Jena and K. Banerjee, Computational Study of Metal Contacts to Monolayer Transition-Metal Dichalcogenide Semiconductors., *Phys. Rev. X*, 2014, **4**(3), 1005–1014.
13 X. D. Duan, C. Wang, A. L. Pan, R. Q. Yu and X. F. Duan, Two-dimensional transition metal dichalcogenides as atomically thin semiconductors: opportunities and challenges, *Chem. Soc. Rev.*, 2015, **44**(24), 8859–8876.

14 M. Tosun, S. Chuang, H. Fang, A. B. Sachid, M. Hettick, Y. Lin, Y. Zeng and A. Javey, High-Gain Inverters Based on WSe_2 Complementary Field-Effect Transistors, *ACS Nano*, 2014, **8**(5), 4948–4953.

15 Z. Y. Ni, M. Ye, J. H. Ma, Y. Y. Wang, R. G. Quhe, J. X. Zheng, L. Dai, D. P. Yu, J. J. Shi, J. B. Yang, S. Watanabe and J. Lu, Performance Upper Limit of sub-10 nm Monolayer MoS_2 Transistors, *Adv. Electron. Mater.*, 2016, **2**(9), 1600191.

16 K. M. McCreary, K. Pi, A. G. Swartz, W. Han, W. Bao, C. N. Lau, F. Guinea, M. I. Katsnelson and R. K. Kawakami, Effect of cluster formation on graphene mobility, *Phys. Rev. B: Condens. Matter Mater. Phys.*, 2010, **81**(11), 115453.

17 C. Sun, H. Xiang, B. Xu, Y. Xia, J. Yin and Z. Liu, *Ab initio* study of carrier mobility of few-layer InSe, *Appl. Phys. Express*, 2016, **9**(3), 035203.

18 S. R. Tamalampudi, Y. Y. Lu, U. R. Kumar, R. Sankar, C. D. Liao, B. K. Moorthy, C. H. Cheng, F. C. Chou and Y. T. Chen, High performance and bendable few-layered InSe photodetectors with broad spectral response, *Nano Lett.*, 2014, **14**(5), 2800–2806.

19 S. Lei, L. Ge, S. Najmaei, A. George, R. Kappera, J. Lou, M. Chhowalla, H. Yamaguchi, G. Gupta, R. Vajtai, A. D. Mohite and P. M. Ajayan, Evolution of the Electronic Band Structure and Efficient Photo-Detection in Atomic Layers of InSe, *ACS Nano*, 2014, **8**(2), 1263–1272.

20 D. A. Bandurin, A. V. Tyurnina, G. L. Yu, A. Mishchenko, V. Zolyomi, S. V. Morozov, R. K. Kumar, R. V. Gorbachev, Z. R. Kudrynskyi, S. Pezzini, Z. D. Kovalyuk, U. Zeitler, K. S. Novoselov, A. Patane, L. Eaves, I. V. Grigorieva, V. I. Fal'ko, A. K. Geim and Y. Cao, High electron mobility, quantum Hall effect and anomalous optical response in atomically thin InSe, *Nat. Nanotechnol.*, 2017, **12**(3), 223–227.

21 D. W. Boukhvalov, B. Gurbulak, S. Duman, L. Wang, A. Politano, L. S. Caputi, G. Chiarello and A. Cupolillo, The Advent of Indium Selenide: Synthesis, Electronic Properties, Ambient Stability and Applications, *Nanomaterials*, 2017, **7**, 11.

22 A. Politano, D. Campi, M. Cattelan, I. B. Amara, S. Jaziri, A. Mazzotti, A. Barinov, B. Gürbulak, S. Duman and S. Agnoli, Indium selenide: an insight into electronic band structure and surface excitations, *Sci. Rep.*, 2017, **7**(1), 3445.

23 I. A. Kibirev, A. V. Matetskiy, A. V. Zotov and A. A. Saranin, Thickness-dependent transition of the valence band shape from parabolic to Mexican-hat-like in the MBE grown InSe ultrathin films, *Appl. Phys. Lett.*, 2018, **112**, 19.

24 M. Wu, J. J. Shi, M. Zhang, Y. M. Ding, H. Wang, Y. L. Cen and J. Lu, Enhancement of photoluminescence and hole mobility in 1- to 5-layer InSe due to the top valence-band inversion: strain effect, *Nanoscale*, 2018, **10**(24), 11441–11451.

25 G. W. Mudd, S. A. Svatek, T. Ren, A. Patane, O. Makarovsky, L. Eaves, P. H. Beton, Z. D. Kovalyuk, G. V. Lashkarev, Z. R. Kudrynskyi and A. I. Dmitriev, Tuning the bandgap of exfoliated InSe nanosheets by quantum confinement, *Adv. Mater.*, 2013, **25**(40), 5714–5718.

26 S. Lei, F. Wen, L. Ge, S. Najmaei, A. George, Y. Gong, W. Gao, Z. Jin, B. Li, J. Lou, J. Kono, R. Vajtai, P. Ajayan and N. J. Halas, An Atomically Layered InSe Avalanche Photodetector, *Nano Lett.*, 2015, **15**(5), 3048–3055.

27 S. Sucharitakul, N. J. Goble, U. R. Kumar, R. Sankar, Z. A. Bogorad, F. C. Chou, Y. T. Chen and X. P. Gao, Intrinsic Electron Mobility Exceeding 10^3 cm^2 V^{-1} s^{-1} in Multilayer InSe FETs, *Nano Lett.*, 2015, **15**(6), 3815–3819.

28 W. Feng, W. Zheng, W. Cao and P. Hu, Back gated multilayer InSe transistors with enhanced carrier mobilities via the suppression of carrier scattering from a dielectric interface, *Adv. Mater.*, 2014, **26**(38), 6587–6593.

29 A. Politano, G. Chiarello, R. Samnakay, G. Liu, B. Gurbulak, S. Duman, A. A. Balandin and D. W. Boukhvalov, The influence of chemical reactivity of surface defects on ambient-stable InSe-based nanodevices, *Nanoscale*, 2016, **8**(16), 8474–8479.

30 Y. Wang, R. Fei, R. Quhe, J. Li, H. Zhang, X. Zhang, B. Shi, L. Xiao, Z. Song, J. Yang, J. Shi, F. Pan and J. Lu, Many-Body Effect and Device Performance Limit of Monolayer InSe, *ACS Appl. Mater. Interfaces*, 2018, **10**(27), 23344–23352.

31 H. Liu, Y. Du, Y. Deng and P. D. Ye, Semiconducting black phosphorus: synthesis, transport properties and electronic applications, *Chem. Soc. Rev.*, 2015, **44**(9), 2732–2743.

32 A. Allain, J. Kang, K. Banerjee and A. Kis, Electrical contacts to two-dimensional semiconductors, *Nat. Mater.*, 2015, **14**(12), 1195–1205.

33 H. Zhong, R. Quhe, Y. Wang, Z. Ni, M. Ye, Z. Song, Y. Pan, J. Yang, L. Yang, M. Lei, J. Shi and J. Lu, Interfacial Properties of Monolayer and Bilayer MoS_2 Contacts with Metals: Beyond the Energy Band Calculations, *Sci. Rep.*, 2016, **6**, 21786.

34 Y. Pan, Y. Wang, M. Ye, R. Quhe, H. Zhong, Z. Song, X. Peng, D. Yu, J. Yang, J. Shi and J. Lu, Monolayer Phosphorene-Metal Contacts, *Chem. Mater.*, 2016, **28**(7), 2100–2109.

35 Y. Pan, Y. Dan, Y. Wang, M. Ye, H. Zhang, R. Quhe, X. Zhang, J. Li, W. Guo, L. Yang and J. Lu, Schottky Barriers in Bilayer Phosphorene Transistors, *ACS Appl. Mater. Interfaces*, 2017, **9**(14), 12694–12705.

36 X. Y. Zhang, Y. Y. Pan, M. Ye, R. Quhe, Y. Y. Wang, Y. Guo, H. Zhang, Y. Dan, Z. G. Song, J. Z. Li, J. B. Yang, W. L. Guo and J. Lu, Three-layer phosphorene-metal interfaces, *Nano Res.*, 2018, **11**(2), 707–721.

37 W. Feng, W. Zheng, X. Chen, G. Liu and P. Hu, Gate Modulation of Threshold Voltage Instability in Multilayer InSe Field Effect Transistors, *ACS Appl. Mater. Interfaces*, 2015, **7**(48), 26691–26695.

38 W. Feng, X. Zhou, W. Q. Tian, W. Zheng and P. Hu, Performance improvement of multilayer InSe transistors with optimized metal contacts, *Phys. Chem. Chem. Phys.*, 2015, **17**(5), 3653–3658.

39 Y. Yuan, R. Quhe, J. Zheng, Y. Wang, Z. Ni, J. Shi and J. Lu, Strong band hybridization between silicene and Ag(111) substrate, *Physica E*, 2014, **58**, 38–42.

40 D. Cheng, G. Barcaro, J.-C. Charlier, M. Hou and A. Fortunelli, Homogeneous Nucleation of Graphitic Nanostructures from Carbon Chains on Ni(111), *J. Phys. Chem. C*, 2011, **115**(21), 10537–10543.

41 C. So, H. Zhang, Y. Wang, M. Ye, Y. Pan, R. Quhe, J. Z. Li, X. Zhang, Y. Zhou and J. Lu, A computational study of monolayer hexagonal WTe_2 to metal interfaces, *Phys. Status Solidi B*, 2017, 1600837.
42 G. Kresse, *ab-initio* Molecular-Dynamics for Liquid-Metals, *J. Non-Cryst. Solids*, 1995, **193**, 222–229.
43 G. Kresse and J. Furthmuller, Efficiency of ab-initio total energy calculations for metals and semiconductors using a plane-wave basis set, *Comput. Mater. Sci.*, 1996, **6**(1), 15–50.
44 H. J. Monkhorst and J. D. Pack, Special Point for Brillouin-Zone Integrations, *Phys. Lett. B*, 1976, **13**(12), 5188–5192.
45 Y. Pan, S. Li, M. Ye, R. Quhe, Z. Song, Y. Wang, J. Zheng, F. Pan, W. Guo, J. Yang and J. Lu, Interfacial Properties of Monolayer $MoSe_2$-Metal Contacts, *J. Phys. Chem. C*, 2016, **120**(24), 13063–13070.
46 M. Brandbyge, J. L. Mozos, P. Ordejon, J. Taylor and K. Stokbro, Density-functional method for nonequilibrium electron transport, *Phys. Rev. B: Condens. Matter Mater. Phys.*, 2002, **65**(16), 5401.
47 D. R. Smith, S. Schultz, P. Markos and C. M. Soukoulis, Determination of effective permittivity and permeability of metamaterials from reflection and transmission coefficients, *Phys. Rev. B: Condens. Matter Mater. Phys.*, 2002, **65**(19), 5104.
48 J. M. Soler, E. Artacho, J. D. Gale, A. Garcia, J. Junquera, P. Ordejon and D. Sanchez-Portal, The SIESTA method for *ab initio* order-N materials simulation, *J. Phys.: Condens. Matter*, 2002, **14**(11), 2745–2779.
49 R. Quhe, S. Feng, J. Lu and M. Lei, Electronic properties of layered phosphorus heterostructures, *Phys. Chem. Chem. Phys.*, 2017, **19**(2), 1229–1235.
50 J. P. Perdew, K. Burke and M. Ernzerhof, Generalized gradient approximation made simple, *Phys. Rev. Lett.*, 1996, **77**(18), 3865–3868.
51 Y. Liang and L. Yang, Carrier plasmon induced nonlinear band gap renormalization in two-dimensional semiconductors, *Phys. Rev. Lett.*, 2015, **114**(6), 063001.
52 R. Quhe, R. Fei, Q. Liu, J. Zheng, H. Li, C. Xu, Z. Ni, Y. Wang, D. Yu, Z. Gao and J. Lu, Tunable and sizable band gap in silicene by surface adsorption, *Sci. Rep.*, 2012, **2**(11), 853.
53 S. Das, W. Zhang, M. Demarteau, A. Hoffmann, M. Dubey and A. Roelofs, Tunable transport gap in phosphorene, *Nano Lett.*, 2014, **14**(10), 5733.
54 H. Jin, J. Li, L. Wan, Y. Dai, Y. Wei and H. Guo, Ohmic contact in monolayer InSe–metal interface, *2D Mater.*, 2017, **4**(2), 5116.
55 Y. Wang, M. Ye, M. Weng, J. Li, X. Zhang, H. Zhang, Y. Guo, Y. Pan, L. Xiao, J. Liu, F. Pan and J. Lu, Electrical Contacts in Monolayer Arsenene Devices, *ACS Appl. Mater. Interfaces*, 2017, **9**(34), 29273–29284.
56 Y. Guo, D. Liu and J. Robertson, 3D Behavior of Schottky Barriers of 2D Transition-Metal Dichalcogenides, *ACS Appl. Mater. Interfaces*, 2015, **7**(46), 25709.
57 J. Li, X. Sun, C. Xu, X. Zhang, Y. Pan, M. Ye, Z. Song, R. Quhe, Y. Wang, H. Zhang, Y. Guo, J. Yang, F. Pan and J. Lu, Electrical contacts in monolayer blue phosphorene devices, *Nano Res.*, 2018, **11**(4), 1834–1849.
58 B. Chamlagain, Q. Li, N. J. Ghimire, H.-J. Chuang, M. M. Perera, H. Tu, Y. Xu, M. Pan, D. Xaio, J. Yan, D. Mandrus and Z. Zhou, Mobility Improvement and Temperature Dependence in $MoSe_2$ Field-Effect Transistors on Parylene-C Substrate, *ACS Nano*, 2014, **8**(5), 5079–5088.
59 D. Krasnozhon, D. Lembke, C. Nyffeler, Y. Leblebici and A. Kis, MoS_2 Transistors Operating at Gigahertz Frequencies, *Nano Lett.*, 2014, **14**(10), 5905–5911.
60 R. Quhe, X. Peng, Y. Pan, M. Ye, Y. Wang, H. Zhang, S. Feng, Q. Zhang, J. Shi, J. Yang, D. Yu, M. Lei and J. Lu, Can a Black Phosphorus Schottky Barrier Transistor Be Good Enough? *ACS Appl. Mater. Interfaces*, 2017, **9**(4), 3959–3966.